

Most Probable Charge of Fission Products in Proton-Induced Fission of ^{238}U and ^{232}Th

D. Kaji,^a S. Goto,^a M. Fujita,^b T. Shinozuka,^b M. Fujioka,^b and H. Kudo^{*,a}

^aDepartment of Chemistry, Faculty of Science, Niigata University, Niigata 950-2181, Japan

^bCyclotron and Radioisotope Center, Tohoku University, Sendai 980-8578, Japan

Received: October 20, 2002; In Final Form: December 6, 2002

The charge distributions of fission products in proton-induced fission of ^{238}U and ^{232}Th were measured in a wide mass range. The most probable charges lay on the proton-rich side in the light fragment region and on the proton-deficient side in the heavy one compared with the unchanged charge distribution hypothesis. This result implies that the charge polarization occurs in the fission process. The charge polarization was examined with respect to the ground-state Q values. The estimations by the Q values fairly well reproduced the experimental most probable charges. These results suggest that the fission path to the most favorable charge division may go through the most energetically favorable path at scission point.

1. INTRODUCTION

Since nuclear fission was discovered, many experiments have been accumulated to reveal the mechanism of fission process. However, no theory has been successful in a complete elucidation of those data. The nuclear charge division of a fissioning nucleus between two fragments results in a charge distribution of fission products. Accordingly, the charge distribution of fission products provides important information about nuclear fission. Many experimental studies have been carried out to determine the charge distribution in various fissioning systems. Wahl et al.¹ proposed that the charge dispersion of fission products in low-energy fission is empirically well represented by a normal Gaussian function which is characterized by two parameters, the most probable charge and the charge dispersion width. These parameters have been discussed for revealing the mechanism of nuclear charge division during fission process. There are some suggestions about the dependence of the width parameter on the excitation energies, fissioning systems, and mass chains.²⁻⁶ Baba et al.⁶ reported that the width of the charge dispersion changes at some incident energy in proton-induced fission of ^{238}U . But the width parameter in α -induced fission of ^{232}Th exhibits no dependence on the excitation energy and is about the same with that in the thermal-neutron-induced fission of ^{235}U .² As for the most probable charge, a few hypotheses have been proposed so far. According to the unchanged charge distribution (UCD) model, primary fission fragments have the same proton-to-mass ratio as in a fissioning nucleus. If the charge in the fissioning nucleus is distributed homogeneously and the redistribution of the charge does not occur in the course of fission process, charge densities of fission fragments will be the same as that of the fissioning nucleus. In this sense, the UCD hypothesis is straightforward and permits a simple method to estimate the most probable charge.⁷⁻⁹ The equal charge displacement (ECD) model states that the most probable charges for one fission fragment and for its complementary fragment lie an equal number of charge units away from the β stability line. This ECD hypothesis was empirically suggested by Glendenin et al.¹⁰ and seems to reproduce the most probable charge in low excitation fission.^{1,11} In the minimum potential energy (MPE) model, a nucleonic redistribution occurs such that a minimum

in the sum of the nuclear potential and Coulomb repulsion energy is attained and fission proceeds along the minimum potential energy surface. This MPE hypothesis was proposed by Present¹² and found to describe the fission of ^{197}Au with 112 MeV ^{12}C rather well.¹³ However, none of these postulates have succeeded in becoming a general rule.

Kudo et al.¹⁴ examined the charge polarization in 24 MeV proton-induced fission of ^{238}U and concluded that the experimental most probable charge was fairly well reproduced by the estimation from production Q values. And it is also reported that some structure in the charge polarization was recognized in the vicinity of $A = 142$ and they attributed it to the deformed shell, $N = 86 - 88$. In order to see whether these findings are the universal evidence, the charge distribution of fission products was measured in the systems of proton-induced fission of ^{238}U and ^{232}Th at various incident energies. The charge distribution is discussed from the view point of charge polarization.

2. EXPERIMENTAL

The experiments were performed by using an azimuthally varying field (AVF) cyclotron and an ion-guide isotope separator on-line (IGISOL) at the Cyclotron and Radioisotope Center in Tohoku University. The Tohoku IGISOL is composed of an ion-guide chamber, a mass separator, and a tape transport system. The details of the Tohoku IGISOL system are described in References 14-16. The ion-guide chamber consists of an ion-guide vacuum chamber and an ion-guide target chamber. The target in the ion-guide target chamber consisted of two self-supported foils of ^{238}U and ^{232}Th in thickness of 20 and 100 mg/cm², respectively. The two targets kept the angle of 45° and 135° with respect to the incident beam direction. The bombarding energies were, 13, 18, and 24 MeV for ^{238}U and 13, 20, and 24 MeV for ^{232}Th at the point between the two target foils. The data for light fragment mass region in the system of 24 MeV proton-induced fission of ^{238}U were re-obtained because of large errors in Reference 14. The beam energy losses in the window foils and target material were evaluated from the range-energy relationship.¹⁷ The beam intensity was monitored by a Faraday cup equipped with a current integrator, and was checked at both the entrance and exit points of the target chamber. The beam current was typically about 2 μA on target.

Mass-separated fission products were collected on an aluminized Mylar tape. The mass calibration was performed at

*Corresponding author. E-mail: hkudo@sc.niigata-u.ac.jp. FAX: +81-25-262-6171.

$A = 16, 32$, and the mass numbers of interest. The mass resolving power M/dM was determined by measuring the γ -ray activities of fission products at each mass number. The typical mass resolving power was about 150.

The radioactivities of fission products collected on the tape were identified and determined by γ -ray spectrometry. Two high-purity germanium (HPGe) detectors coupled with 4096-channel pulse height analyzers were used for the detection of γ -radiations. One detector was positioned just behind the collecting point of transported fission products and used for the measurement of accumulating radioactivities. The other was set about 38 cm away from the first detector along the collection tape and used for a growth and decay measurement. It took 0.6 s to move the collection tape between the two measuring positions. The time interval of the tape transportation was varied from 5 s to 30 min according to the half-lives of the nuclides of interest. In order to reduce statistical errors, the counting cycle was repeated appropriate times. In order to avoid the counting loss from the photopeak through coincidence summing, the detectors were placed at positions which are more than 2 cm away from the source positions. The typical energy resolutions (FWHM) of the two HPGe detectors were 2.1 and 2.8 keV for 1332 keV γ -ray of ^{60}Co , respectively. The energy and efficiency calibrations for γ -ray energy range from 50 to about 2500 keV were performed using a set of γ -ray reference sources (^{133}Ba , ^{57}Co , ^{137}Cs , ^{54}Mn , ^{22}Na , and ^{60}Co) of Amersham, a mixed radionuclide γ -ray reference sources of Amersham (containing ^{108}Cd , ^{57}Co , ^{139}Ce , ^{208}Hg , ^{113}Sn , ^{85}Sr , ^{137}Cs , ^{88}Y , and ^{60}Co), and handmade sources of ^{56}Co and of ^{152}Eu . The γ -ray spectral data were recorded event by event together with time information.

The charge distribution of fission products in 13 and 20 MeV proton-induced fission of ^{232}Th was also measured by a direct collection technique. In this measurement, ^{232}Th targets were prepared by electrodeposition onto a 6.7 mg/cm² thick aluminum backing foil from an isopropanol solution. The thickness of each target was about 500 $\mu\text{g}/\text{cm}^2$ and the precise amount of ^{232}Th was determined by α spectrometry with a surface barrier detector of a known counting efficiency. The obtained ^{232}Th targets were wrapped with 6.7 mg/cm² thick aluminum cover foils for a complete collection of fission products. Two of the wrapped targets were stacked for irradiations. Irradiations were carried out with the proton beams from the JAERI tandem Van de Graaff accelerator. The proton energy in each target was calculated from the range-energy relationship.¹⁷ Beam intensity was monitored with a Faraday cup during the irradiation. The beam intensity from the accelerator was in the range of 0.3 to 0.4 μA . The irradiation duration was 5 min for short-lived products and 30 min for long-lived ones. The radioactivities of fission products were identified and determined by γ -ray spectrometry.

3. RESULTS AND DISCUSSION

The obtained radioactivities were converted to either cumulative yields or independent yields as follows. After the end of collection, the radioactivities of the members of a given decay chain at time t are given by

$$A_1 = A_{10} \exp(-\lambda_1 t) \quad (1)$$

$$A_2 = A_{10} \frac{\lambda_2}{\lambda_2 - \lambda_1} \{ \exp(-\lambda_1 t) - \exp(-\lambda_2 t) \} + A_{20} \exp(-\lambda_2 t) \quad (2)$$

...

where A_{10}, A_{20}, \dots are the activities at the end of collection. The obtained activities at the end of collection were converted to corresponding cross sections by correcting for saturation conditions. The next differential equations hold during the period of collection.

$$\frac{dN_1}{dt} = N_0 \sigma_1 \varepsilon_1 \phi - N_1 \lambda_1 \quad (3)$$

$$\frac{dN_i}{dt} = N_0 \sigma_i \varepsilon_i \phi + N_{i-1} \lambda_{i-1} - N_i \lambda_i \quad (4)$$

$$i = 2, 3, \dots$$

where N_0 is the number of target nuclei, σ_i is the cross section, ε_i is the transport efficiency in IGISOL, and ϕ is the proton beam flux. These differential equations can be easily solved and the relative yields in the form of $N_0 \sigma_i \varepsilon_i$ are obtained by substituting A_{i0} 's in eqs 1 and 2 for the resulting equations. The transport efficiency may be affected by both the operating conditions of the mass separator and the chemical properties of elements. But the differences in transport efficiencies can be eliminated by taking an appropriate ratio of the obtained yields as described in Reference 14. The measured nuclides and the nuclear data used for the analysis are summarized in Table 1 with quated References 18–54.

Empirically, the charge dispersion of fission products has been well represented by a Gaussian function.¹ The theoretical calculations with the asymmetric two-center shell model^{55, 56} and the statistical model by Fong et al.⁵⁷ also give a Gaussian function. At low energy fission, a certain deviation from the Gaussian curve was observed because of an odd-even effect.⁴ But in a charged-particle-induced fission, the odd-even effect is presumed not to appear because high excitation energy of fissioning nuclei washes out the effect. It is reported that the odd-even effect is reduced when an extra 3 MeV is added to the system of neutron-induced fission of ^{238}U .⁵⁸ Therefore, the analysis of the charge dispersion was performed assuming the following function

$$P(A, Z) = \frac{P(A)}{\sqrt{\pi}C} \exp\left\{-\frac{(Z-Z_p)^2}{C}\right\}, \quad (5)$$

where $P(A, Z)$ is the independent yield of the nuclide with an atomic number Z and a mass number A , P is the chain yield of the mass chain A , Z_p is the most probable charge, and C is the width parameter of the charge dispersion.

There are several indications about the dependence of the width parameter on the excitation energies, fissioning systems, and mass chains. Baba et al.⁶ reported that the charge dispersion width in proton-induced fission of ^{238}U changes with the incident-proton energy. On the other hand, there are also contrary evidences that the width parameter is independent of the excitation energies. For example, McHugh and Michel² indicated that the fractional yield data of ^{135}I , ^{135}Xe , and ^{135}Cs obtained in α -induced fission of ^{232}Th with the various excitation energies up to 39 MeV are well represented with a single charge dispersion curve. The value of C that best fits all energies was 0.95 ± 0.05 . This value was quite similar to the value, $C = 0.94 \pm 0.15$, determined in thermal-neutron-induced fission of ^{235}U .^{3, 4} Since the same compound nucleus ($^{236}\text{U}^*$) was produced in both systems, the above results indicate that a single charge dispersion function is maintained through a wide range of excitations. Umezawa⁵⁹ reported that the charge dispersion is identical for all investigated mass chains obtained in the system of proton-induced fission of ^{238}U . Besides, Blann¹³ has reported that the width of the charge dispersion curve is 0.9 ± 0.1 in the fission of gold with 112 MeV ^{12}C ions. These results suggest that the width of the charge dispersion is identical for any mass chains in various fissioning systems. In the present analysis, the width parameter is assumed to be independent of excitation energies, mass numbers, and fissioning systems investigated. If more than two same Z nuclides of mass number, A , are observed at different proton-energies, E_1 and E_2 , the difference of the most probable charges between E_1 and E_2 can be expressed as follows

TABLE 1: Nuclear Data Used for the Analysis Only a Main Characteristic Gamma Ray of Each Nuclide is Listed

Nuclide	T _{1/2}	E _γ /keV	I _γ %	Ref. type ^{a)}	Nuclide	T _{1/2}	E _γ /keV	I _γ %	Ref. type ^{a)}	Nuclide	T _{1/2}	E _γ /keV	I _γ %	Ref. type ^{a)}	Nuclide	T _{1/2}	E _γ /keV	I _γ %	Ref. type ^{a)}		
⁸² Ge	4.6 s	1091.9	90	[18] C	^{99m} Nb	2.6 min	253.3	3.71 [29] I		^{124b} In	2.4 s	1359.9	38.8 [38] I		^{138m} Cs	2.9 min	191.7	15.4 [44] I			
^{82b} As	13.6 s	343.5	57.6 [18] I		^{99b} Nb	15 s	137.7	90.6 [29] I		^{124a} In	3.17 s	997.8	21.1 [38] I		^{138g} Cs	32.2 min	1009.8	29.8 [44] I			
^{82a} As	19.1 s	654.4	15.1 [18] I		¹⁰¹ Mo	14.61 m	590.9	15.66 [30] C		¹²⁶ Cd	0.51 s	260.1	89.6 [39] C		¹³⁹ Xe	39.68 s	218.6	52 [45] C			
⁸⁴ As	5.5 s	1455.1	49 [19] C		¹⁰¹ Tc	14.22 m	306.8	88 [30] I		^{126b} In	1.45 s	111.8	88 [39] I		¹³⁹ Cs	9.27 min	1283.2	7.7 [45] I			
⁸⁴ Ge	3.1 min	408.2	100 [19] I		¹⁰² Mo	11.2 min	211.7	3.82 [22] C		^{126a} In	1.5 s	969.6	14.9 [39] I		¹³⁹ Ba	1.38 h	165.8	23.8 [45] I			
^{84m} Br	6 min	424	100 [19] I		^{102m} Tc	4.35 min	628.1	25.2 [22] I		^{128b} In	0.9 s	1867	32.3 [40] C		¹³⁹ Xe	13.6 s	805.5	20 [46] C			
^{84g} Br	31.8 min	1897.6	14.7 [19] I		^{102g} Tc	5.28 s	475.1	6.25 [22] I		^{128a} In	0.9 s	1168.8	50.3 [40] C		¹⁴⁰ Cs	63.7 s	908.4	7.89 [46] I			
⁸⁸ Se	1.52 s	159.2	10.6 [20] C		¹⁰⁵ Tc	7.6 m	143.3	15.7 [31] C		^{128m} Sn	6.5 s	831.5	100 [40] I		¹⁴¹ Xe	1.73 s	909.4	13.3 [47] C			
⁸⁸ Br	16.5 s	775.3	63 [20] I		¹⁰⁵ Ru	4.44 h	469.7	17.55 [31] I		^{128g} Sn	59.1 min	482.3	58 [40] I		¹⁴¹ Cs	24.94 s	561.6	4.7 [47] I			
⁸⁸ Kr	2.84 h	196.3	26 [20] I		¹⁰⁷ Ru	3.75 m	194.1	9.85 [32] C		^{128b} Sb	10.4 min	314	91.6 [40] I		¹⁴¹ Ba	18.27 min	190.3	47 [47] I			
⁸⁸ Rb	17.78 min	1836	21.4 [20] I		¹⁰⁷ Rh	21.7 m	302.8	66 [32] I		^{128g} Sb	9.01 h	526.5	45 [40] I		¹⁴² Ba	10.6 min	255.3	21.1 [48] C			
⁸⁹ Kr	3.15 m	586	16.6 [21] C		¹⁰⁸ Tc	5.17 s	242.2	82.4 [33] C		^{130m} Sn	1.7 min	144.9	34 [22] C		¹⁴² La	91.1 min	641.3	47.4 [48] I			
⁸⁹ Rb	15.15 m	1248.1	42.6 [21] I		¹⁰⁸ Ru	4.55 min	(434.1 43.3) ^{b)}	[33] I		^{130g} Sn	3.72 min	192.5	71 [22] I		¹⁴³ Cs	1.78 s	195.5	12.6 [49] C			
⁹⁰ Br	1.92 s	707.1	38 [22] C		^{108b} Rh	6 min	581.1	59 [33] I		^{130b} Sb	6.3 min	1017.5	30 [22] I		¹⁴³ Ba	14.5 s	211.5	24.9 [49] I			
⁹⁰ Kr	32.3 s	1118.7	36.2 [22] I		^{108g} Rh	16.8 s	434.1	43 [33] I		^{130a} Sb	40 min	330.9	78 [22] I		¹⁴³ La	14.2 min	643.7	1.55 [49] I			
^{90m} Rb	4.3 min	824.2	8.64 [22] I		¹¹⁶ Pd	12.72 s	114.7	88 [22] C		^{130m} I	9 min	536.1	16.7 [22] I		¹⁴³ Ce	33 h	293.3	42.8 [49] I			
^{90b} Rb	2.6 min	831.7	27.8 [22] I		^{116m} Ag	10.4 s	1028.9	30 [22] I		^{130g} I	12.36 h	668.5	96.1 [22] I		¹⁴⁴ Ba	11.5 s	388.2	13.5 [50] C			
⁹¹ Kr	8.57 s	108.8	43.5 [23] C		^{116g} Ag	2.68 min	699.3	10.9 [22] I		¹³² Sn	40 s	340.8	43.2 [22] C		¹⁴⁴ La	40.8 s	397.4	94.3 [50] I			
⁹¹ Rb	58.4 s	93.6	33.7 [23] I		^{116m} In	2.18 s	162.4	36.6 [22] I		^{132b} Sb	2.8 min	989.6	15 [22] I		¹⁴⁵ Cs	0.594 s	175.4	15.6 [51] C			
⁹¹ Sr	9.52 h	1024.3	33.4 [23] I		^{116m} In	54.15 min	416.9	26.2 [22] I		^{132a} Sb	4.2 min	1041.5	18 [22] I		¹⁴⁵ Ba	4.31 s	96.6	7.73 [51] I			
⁹² Kr	1.85 s	142.4	66 [24] C		¹¹⁹ Ag	2.1 s	626.4	10.7 [22] C		¹³² Te	78.2 h	228.2	88.1 [22] I		¹⁴⁵ La	24.8 s	355.8	3.83 [51] I			
⁹² Rb	4.5 s	814.7	8 [24] I		^{119m} Cd	2.2 min	1025	25 [22] I		^{132m} I	83.6 min	599.8	13.2 [22] I		¹⁴⁵ Ce	3.01 min	724.2	58.9 [51] I			
⁹² Sr	2.71 h	1383.9	90 [24] I		^{119g} Cd	2.69 min	292.9	41 [22] I		¹³² I	2.3 h	522.7	16.1 [22] I		¹⁴⁶ Ba	2.2 s	251.2	18 [52] C			
⁹² Y	3.54 h	934.5	13.9 [24] I		¹²⁰ Cd	50.8 s	(1172.5 20.3) ^{b)}	[34] C		¹³⁴ Te	41.8 min	210.5	22.5 [41] C		^{146m} La	10 s	409.9	87 [52] I			
⁹³ Kr	1.29 s	266.8	20.3 [25] C		^{120b} In	47.3 s	89.9	77.6 [34] I		^{134m} I	3.69 min	271.9	79 [41] I		^{146g} La	6.27 s	258.5	76 [52] I			
⁹³ Rb	5.7 s	986.2	4.43 [25] I		^{120b} In	46.2 s	863.7	32.5 [34] I		^{134g} I	52.6 min	1072.5	15 [41] I		¹⁴⁶ Ce	13.52 min	316.7	51 [52] I			
⁹³ Sr	7.423 min	590.3	65.7 [25] I		^{120g} In	3.08 s	1172.5	19 [34] I		¹³⁵ Te	19 s	603.5	37 [42] C		¹⁴⁶ Pr	24.15 min	453.9	48 [52] I			
⁹⁴ Rb	2.702 s	836.9	87.1 [26] C		¹²¹ Ag	0.72 s	341.6	30.9 [35] C		¹³⁵ I	6.57 h	1260.4	28.9 [42] I		¹⁴⁷ La	4.48 s	117.6	15 [22] C			
⁹⁴ Sr	75.1 s	1427.6	94.2 [26] I		^{121m} Cd	8.3 s	1020.9	18.9 [36] I		^{135m} Xe	15.29 min	526.6	80.5 [42] I		¹⁴⁷ Ce	56.4 s	268.7	5.5 [22] I			
⁹⁵ Sr	25.1 s	685.9	24 [27] C		^{121g} Cd	13.5 s	324.2	49.5 [36] I		^{135g} Xe	9.14 h	249.8	90.2 [42] I		¹⁴⁸ La	1.05 s	158.5	56 [53] C			
⁹⁵ Y	10.3 min	954.2	19 [27] I		¹²⁴ In	23.1 s	925.6	87 [22] I		¹³⁶ Te	17.5 s	334	18.8 [43] C		¹⁴⁸ Ce	56 s	269.5	17 [53] I			
⁹⁷ Sr	0.42 s	1905	28 [28] C		¹²² Cd	5.24 s	1140.3	39 [37] C		^{136b} I	46.9 s	381.4	99.8 [43] I		^{148m} Pr	2 min	450.8	50 [53] I			
^{97m} Y	1.23 s	161.4	70.7 [28] I		^{122a} In	10.8 s	407.3	7.8 [37] I		^{136a} I	83.4 s	1321.1	24.8 [43] I		^{148g} Pr	2.27 min	301.7	61 [53] I			
^{97b} Y	3.5 s	3287.7	18.1 [28] I		^{122b} In	10.3 s	1190.3	20 [37] I		¹³⁶ Cs	13.16 d	818.5	99.7 [43] I		¹⁴⁹ Pr	2.26 min	138.5	1.02 [54] C			
⁹⁹ Y	1.47 s	121.8	43.8 [29] C		^{122a} In	1.5 s	1013.1	2.7 [37] I		¹³⁸ I	6.41 s	588.8	60 [44] C		¹⁴⁹ Nd	1.72 h	211.3	25.9 [54] I			
⁹⁹ Zr	2.1 s	469.1	55.2 [29] I		¹²⁴ Cd	0.9 s	179.9	49.9 [38] C		¹³⁸ Xe	14.08 min	258.4	31.5 [44] I								

a) C: cumulative yield, I: independent yield
b) Used daughter activity

$$dZ_P(\text{Energy}) \equiv Z_P(E_1) - Z_P(E_2)$$

$$= \frac{C}{2(Z_1 - Z_2)} \ln \left\{ \frac{P_{E1}(A, Z_1) \cdot P_{E2}(A, Z_2)}{P_{E1}(A, Z_2) \cdot P_{E2}(A, Z_1)} \right\}, \quad (6)$$

Similarly, if more than two identical nuclides at different targets, ²³²Th and ²³⁸U, are observed, the difference can be expressed by the following function

$$dZ_P(\text{Target}) \equiv Z_P(\text{Th}) - Z_P(\text{U})$$

$$= \frac{C}{2(Z_1 - Z_2)} \ln \left\{ \frac{P_{Th}(A, Z_1) \cdot P_U(A, Z_2)}{P_{Th}(A, Z_2) \cdot P_U(A, Z_1)} \right\}, \quad (7)$$

As a result, the $dZ_P(\text{Energy})$ and $dZ_P(\text{Target})$ were given in a unit of the width parameter C . So far, the most probable charge was precisely reported in the 24 MeV proton-induced fission of ²³⁸U,¹⁴ where the value of the width parameter was given as 1.00 ± 0.12 . The most probable charges for other systems were evaluated by converting the obtained data using eqs 6 and 7. The resulting information is based on their differences, but the transport efficiency in IGISOL is eliminated. In the course of the analysis, the width parameter was intentionally varied from 0.90 to 1.10, but the most probable charges were almost unaffected with variation of the width parameter. In the case of the direct collection technique, 13 and 20 MeV proton-induced fission of ²³²Th, the most probable charges were directly obtained using a fixed width parameter, $C = 1.00$. Mass distributions calculated with these parameters well agreed with reported ones.⁶⁰ Therefore, the most probable charges obtained in the present work can be regarded as reasonable ones. The evaluated most probable charges are plotted against the product mass number in Figure 1. The linear broken lines depicted in the figure show the most probable charge expected from the unchanged charge distribution (UCD) hypothesis. According to the UCD hypothesis, the primary fission fragments have the same proton-to-mass ratio of the fissioning nucleus.

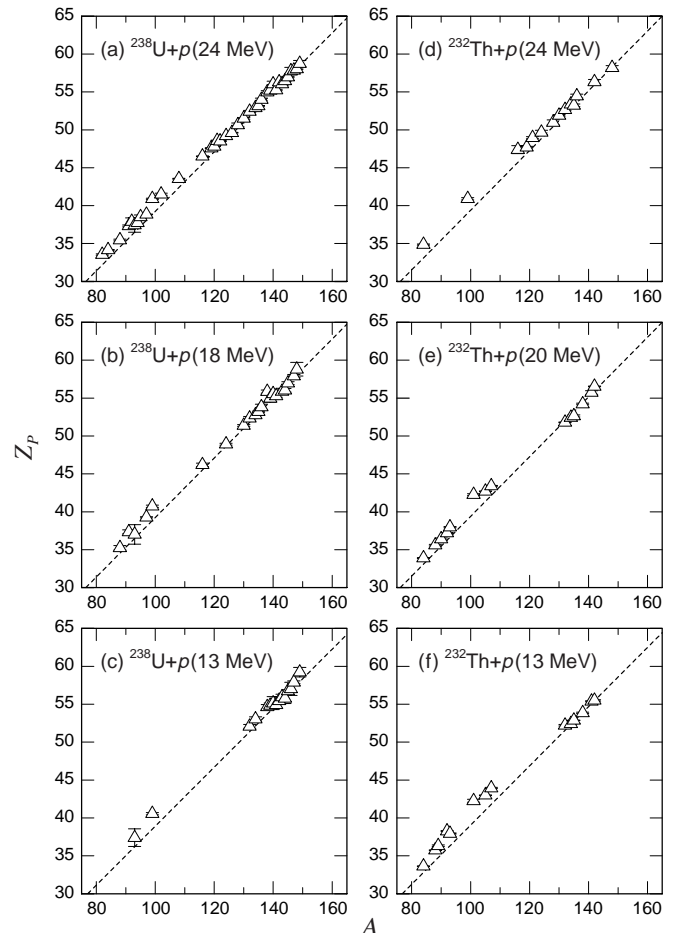


Figure 1. The most probable charge, Z_P , plotted as a function of product mass number, A . The linear broken line shows the most probable charge expected from the unchanged charge distribution hypothesis.

The fissioning nuclei were assumed to be ^{239}Np for the 13 MeV $p + ^{238}\text{U}$ system, ^{237}Np for the 18 and 24 MeV $p + ^{238}\text{U}$ systems,⁶¹ ^{233}Pa for the 13 MeV $p + ^{232}\text{Th}$ system, and ^{231}Pa for the 20 and 24 MeV $p + ^{232}\text{Th}$ systems.⁶⁰ The most probable charges gradually increase with an increase of the fragment mass number in all the systems. It is necessary to elucidate masses of primary fragments for the precise comparison. The primary fragment mass can be estimated by adding the number of emitted neutrons, ν , but they were reported only in a limited number of systems. In the present analysis, the correction for the emitted neutrons was performed by using the data of 12.7, 22.0, and 25.5 MeV^{62, 63} for the 13, 18, and 24 MeV $p + ^{238}\text{U}$ systems, respectively. And for the 13, 20, and 24 MeV $p + ^{232}\text{Th}$ systems, the data of 13.2, 14.7, and 14.7 MeV,⁶⁴ respectively, were used. The comparison revealed the distinct deviation of the experimental Z_p from the charge expected from UCD, Z_{UCD} . The deviations of Z_p from Z_{UCD} are displayed as a function of the fragment mass number, A' , in Figure 2. As seen in the figure, Z_p 's mainly lay on the proton-rich side in the light fragment mass region and on the neutron-rich side in the heavy mass region in all the systems. These results imply that the charge polarization occurs in fission process. The nuclides of higher charge density are formed in the light fragment region, while those of lower charge density are produced in the heavy fragment region compared with the UCD hypothesis. As the neutron-to-proton ratio of stable nuclei increases with an increase of the mass number, the present results suggest that the nuclear stability of fission fragments reflects the charge polarization in fission.

The deviation of Z_p of the complementary fragment from the corresponding Z_{UCD} should be the same but with an opposite sign because the probability of charged particle emission is quite small in low energy fission. This can be ascertained by superimposing the complementary light fragments to the heavy ones. The results are shown in Figure 3, where the primary

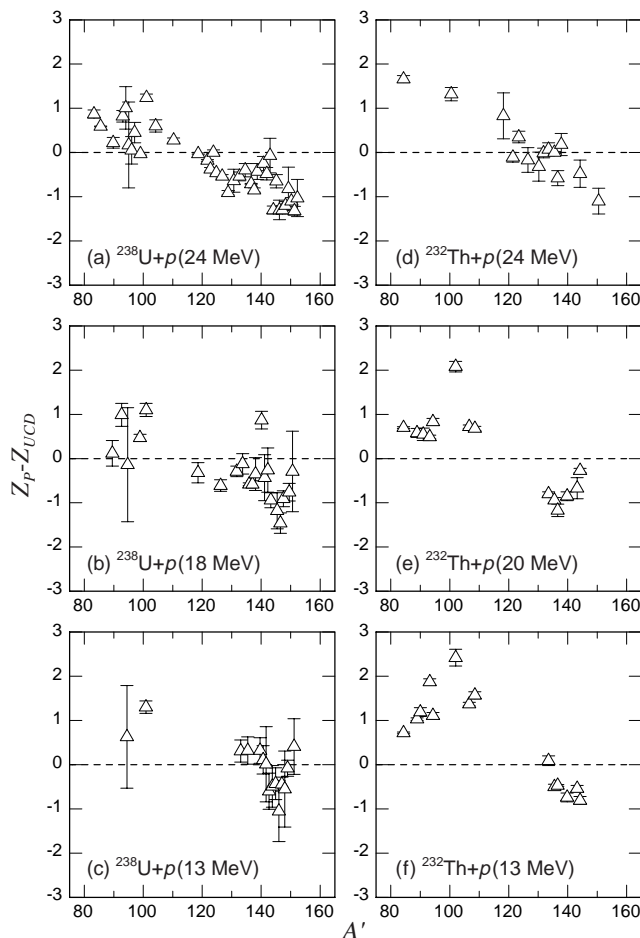


Figure 2. Deviation of Z_p from Z_{UCD} plotted versus primary fragment mass number, A' .

heavy fragment mass number, A_h' , is taken as an abscissa. The deviations of the complementary fragments are nearly consistent. These results indicate that the most probable charge is not seriously affected by neutron emission from fission fragments.

For a given mass split, many combinations of charge division are possible. The most probable charge was examined in connection with the most energetically favorable combination. The most energetically favorable charge, Z_{Qgg} , was estimated by the ground-state Q value as in Reference 14. In this estimation, the Q value was defined as the difference between the mass of the fissioning nucleus and the ground-state masses of fission fragments.^{65, 66} The results are shown in Figure 3 by solid curves. The experimental Z_p seems to agree with the evaluated Z_{Qgg} in the systems of 18 MeV protons on ^{238}U , 24 MeV protons on ^{238}U , and 20 MeV protons on ^{232}Th . But the agreement between the experimental and evaluated Z_p 's is not good in the case of other systems showed in Figures 3(c), 3(d), and 3(f). The data in Figure 3(c) and 3(f) are for the lowest proton-energy studied in the present work. The effect such as shell effect, which is emphasized in low energy region, may influence of the most probable charge. For example, in $A = 135$ the charge of nuclide with $N = 82$ shell is larger than Z_{Qgg} . As the yield of nuclide with $N = 82$ shell may be enhanced, the most probable charge increases and consequently deviates from Z_{Qgg} . The same kind of explanation is applicable to the disagreement at other nuclear shell and deformed shell, $N = 86-88$, which is suggested by Wilkins et al.⁶⁷ The existence of the nuclear shell effect in this energy region was also reported in the isomeric yield ratio measurement.⁶⁸ On the other hand, the reason why Z_p dose not seem to agree with Z_{Qgg} in the 24 MeV proton + ^{232}Th system is probably because of the inadequate correction of emitted neutrons.

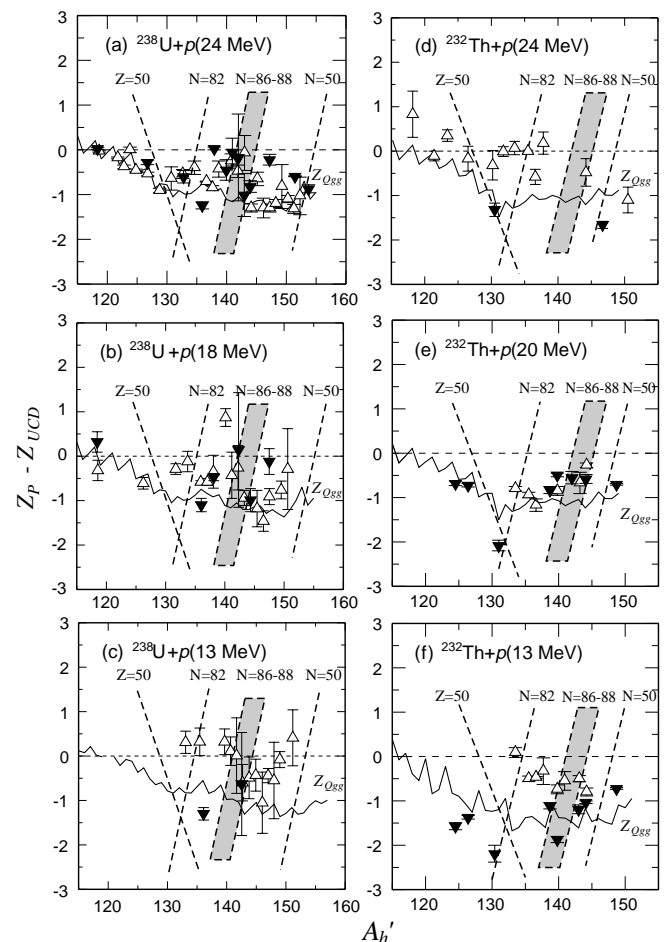


Figure 3. Same as Figure 2, but folded at the symmetric mass with superimposing the complementary light fragments. The light mass products are indicated by closed symbols. The solid curve is the result of the estimation by using production Q values.

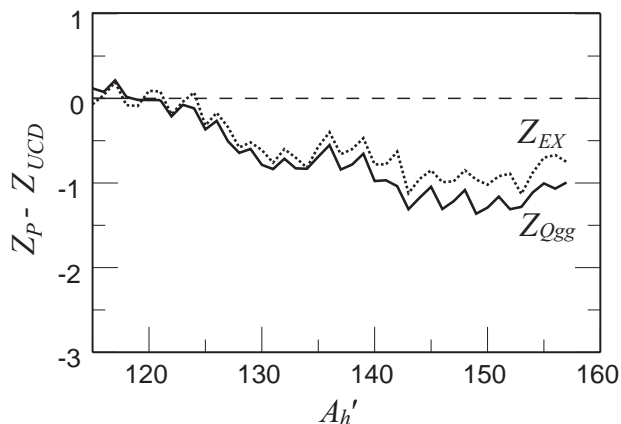


Figure 4. Comparison of Z_{OGG} estimated from ground state masses with Z_{EX} estimated by considering deformation at scission for the fissioning nucleus of ^{239}Np .

Because the number of the emitted neutrons were not reported for 24 MeV proton-induced fission of ^{232}Th , we used the data of the 14.7 MeV protons on ^{232}Th . The dependence of ν on the excitation energy was demonstrated by Bishop et al.⁶² and by Strecker et al.,⁶³ and according to them, there are two striking features. The first one is the disappearance of the sawtooth structure with increasing excitation energy. The other one is the tendency for ν to increase more rapidly with an increase of excitation energy for heavier fragment than for the light fragment, even in the mass region away from closed shells. If the dependence of ν on excitation energy for the $^{232}\text{Th} + p$ system is similar to that for the $^{238}\text{U} + p$ system, Z_p is expected to approach to Z_{OGG} in Figure 3(d).

If the shape of the β stability vs. nuclear charge curve at a given mass number is about the same for the complementary fragment pair, the maximum energy is available for the pair at which the differences between the most stable charge and the fragment charge are the same. In this sense, the ECD model has the similar meaning as the present consideration by the Q values.

It is generally considered that fission fragments are highly deformed at scission point. Accordingly the masses at scission point are expected to be different from the ground-state masses and the explanation by the ground-state masses seems to be unrealistic. As the deformation at scission point is not well understood, two-spheroid model by Quentin⁶⁹ was assumed for scission point configuration. Assuming that the degrees of the deformation of complementary fragments are the same and that the kinetic energy, TKE, of fission fragments is purely originated from the Coulomb repulsion between two fragments at scission, the deformation energy at scission was calculated after the method of Brossa et al.⁷⁰ The values of TKE presented by Strecker et al.⁶³ for proton-induced fission of ^{238}U and by Croall and Cuninghame⁷¹ for proton-induced fission of ^{232}Th were used in the calculation. For a given mass split, the deformation energies, E_{def} , at scission point were calculated with varying combinations of charge division. The charge expected from the most energetically favorable combinations at scission point, Z_{EX} , was determined from the largest $(Q - E_{def})$ for a given mass split. It was found that Z_{EX} is not largely different from Z_{OGG} . An example of the results is shown in Figure 4 for the fissioning nucleus of ^{239}Np . This result indicates that the ground-state masses can be used for the estimation of the most energetically favorable charge.

4. CONCLUSIONS

The charge distributions of fission products were measured in the systems of 13, 18, and 24 MeV proton-induced fission of ^{238}U and of 13, 20, and 24 MeV proton-induced fission of

^{232}Th . A large number of these data enabled to get much information on the most probable charge, Z_p . In all the systems studied, Z_p 's mainly lay on the proton-rich side in the light fragment mass region and on the proton-deficient side in the heavy mass region, that is, the nuclides of higher charge density formed in the light fragment region and those of lower charge density produced in the heavy fragment region. These results imply that the charge polarization occurs in the fission process and that the nuclear stability of fission fragments reflects the charge polarization in fission. The charge polarization was examined with respect to the ground-state Q values. The experimental Z_p was fairly well reproduced by the estimation by the Q values except for the system of 13 MeV proton-induced fission of ^{238}U and ^{232}Th . These results suggest that the fission path to the most favorable charge division may go through the most energetically favorable path.

Acknowledgements. The authors wish to express their acknowledgement to the crews of cyclotron of Tohoku University and JAERI tandem accelerator for splendid operation. Thanks are due to Dr. Y. Nagame, Dr. K. Tsukada, and Dr. S. Ichikawa of JAERI for the help in a part of the measurements.

References

- (1) A. C. Wahl, R. L. Ferguson, D. R. Nethaway, D. E. Troutner, and K. Wolfsberg, *Phys. Rev.* **126**, 1112 (1962).
- (2) J. A. McHugh and M. C. Michel, *Phys. Rev.* **172**, 1160 (1968).
- (3) A. C. Wahl, *J. Radioanal. Chem.* **55**, 111 (1980).
- (4) A. C. Wahl, *At. Data Nucl. Data Tables* **39**, 1 (1988).
- (5) G. R. Choppin and E. F. Meyer, Jr., *J. Inorg. Nucl. Chem.* **28**, 1509 (1966).
- (6) H. Baba, A. Yokoyama, N. Takahashi, N. Nitani, R. Kasuga, T. Yamaguchi, D. Yano, K. Takamiya, N. Shinohara, K. Tsukada, Y. Hatsukawa, and Y. Nagame, *Z. Phys. A* **356**, 61 (1996).
- (7) R. H. Goeckermann and I. Perlman, *Phys. Rev.* **76**, 628 (1949).
- (8) G. Friedlander, L. Friedman, B. Gordon, and L. Yaffe, *Phys. Rev.* **129**, 1809 (1963).
- (9) J. H. Davies and L. Yaffe, *Can. J. Phys.* **41**, 762 (1963).
- (10) L. E. Glendenin, C. D. Coryell, and R. E. Edwards, *Radiochemical Studies: The fission products* (McGraw-Hill, New York, 1951).
- (11) A. C. Pappas, Paper P/881, *Proceedings of the International Conference on the Peaceful Uses of Atomic Energy*, Geneva, 1995.
- (12) R. D. Present, *Phys. Rev.* **72**, 7 (1947).
- (13) H. M. Blann, *Phys. Rev.* **123**, 1356 (1961).
- (14) H. Kudo, M. Maruyama, M. Tanikawa, T. Shinozuka, and M. Fujioka, *Phys. Rev. C* **57**, 178 (1998).
- (15) M. Yoshii, H. Hama, K. Taguchi, T. Ishimatsu, T. Shinozuka, M. Fujioka, and J. Årje, *Nucl. Instr. Meth. B* **26**, 410 (1987).
- (16) H. Kudo, M. Maruyama, M. Tanikawa, M. Fujita, T. Shinozuka, and M. Fujioka, *Nucl. Instr. Meth. B* **126**, 209 (1997).
- (17) J. F. Janni, *At. Data Nucl. Data Tables* **27**, 147 (1982).
- (18) H. W. Müller, *Nucl. Data Sheets* **50**, 1 (1987).
- (19) H. W. Müller, *Nucl. Data Sheets* **56**, 551 (1989).
- (20) H. W. Müller, *Nucl. Data Sheets* **54**, 1 (1988).
- (21) H. Sievers, *Nucl. Data Sheets* **58**, 351 (1989).
- (22) U. Reus and W. Westmier, *At. Data and Nucl. Data Tables Part 2* **29**, 193 (1983).
- (23) H. W. Müller, *Nucl. Data Sheets* **31**, 181 (1980).
- (24) P. Luksch, *Nucl. Data Sheets* **30**, 573 (1980).
- (25) H. Sievers, *Nucl. Data Sheets* **54**, 99 (1988).

- (26) H. W. Müller, Nucl. Data Sheets **44**, 277 (1985).
(27) P. Luksch, Nucl. Data Sheets **38**, 1 (1983).
(28) B. Haesner and P. Luksch, Nucl. Data Sheets **46**, 607 (1985).
(29) H. W. Müller and D. Chielewska, Nucl. Data Sheets **48**, 663 (1986).
(30) J. Blachot, Nucl. Data Sheets **45**, 701 (1985).
(31) D. De Frenne, E. Jacobs, M. Verboven, and P. De Gelder, Nucl. Data Sheets **47**, 261 (1986).
(32) J. Blachot, Nucl. Data Sheets **62**, 709 (1991).
(33) R. L. Haese, F. E. Bertland, B. Harmatz, and M. J. Martin, Nucl. Data Sheets **37**, 289 (1982).
(34) A. Hashizume, Y. Tendow, and M. Ohsha, Nucl. Data Sheets **52**, 641 (1987).
(35) B. Fogelberg and P. Hoff, Nucl. Phys. A **391**, 445 (1982).
(36) B. Fogelberg and P. Hoff, Nucl. Phys. A **376**, 389 (1982).
(37) K. Kitao, M. Kanbe, Z. Matsumoto, and T. Seo, Nucl. Data Sheets **49**, 315 (1986).
(38) T. Tamura, K. Miyano, and S. Ohya, Nucl. Data Sheets **41**, 413 (1984).
(39) T. Tamura, K. Miyano, and S. Ohya, Nucl. Data Sheets **36**, 227 (1982).
(40) K. Kitao, M. Kanbe, and Z. Matsumoto, Nucl. Data Sheets **38**, 191 (1983).
(41) Yu. V. Sergeenkov and V. M. Sigalov, Nucl. Data Sheets **34**, 475 (1981).
(42) Yu. V. Sergeenkov, Nucl. Data Sheets **52**, 205 (1987).
(43) T. W. Burrows, Nucl. Data Sheets **52**, 273 (1987).
(44) L. K. Peker, Nucl. Data Sheets **36**, 289 (1982).
(45) L. K. Peker, Nucl. Data Sheets **32**, 1 (1981).
(46) L. K. Peker, Nucl. Data Sheets **51**, 425 (1987).
(47) L. K. Peker, Nucl. Data Sheets **45**, 1 (1985).
(48) L. K. Peker, Nucl. Data Sheets **43**, 579 (1984).
(49) L. K. Peker, Nucl. Data Sheets **48**, 753 (1986).
(50) J. K. Tuli, Nucl. Data Sheets **56**, 607 (1989).
(51) L. K. Peker, Nucl. Data Sheets **49**, 1 (1986).
(52) L. K. Peker, Nucl. Data Sheets **41**, 195 (1984); B. Sohnius, M. Brugger, H. O. Denschlag, and B. Pfeiffer, Radiochim. Acta **37**, 125 (1984).
(53) L. K. Peker, Nucl. Data Sheets **42**, 111 (1984).
(54) J. A. Sziucs, M. W. John, and B. Singh, Nucl. Data Sheets **46**, 1 (1985).
(55) R. K. Gupta, W. Scheild, and W. Greiner, Phys. Rev. Lett. **35**, 353 (1975).
(56) D. R. Saroha, R. Aroumougame, and R. K. Gupta, Phys. Rev. C **27**, 2720 (1983).
(57) P. Fong, Phys. Rev. **103**, 434 (1956).
(58) J. P. Bocquet and R. Brissot, Nucl. Phys. A **560**, 213c (1989).
(59) H. Umezawa, J. Inorg. Nucl. Chem. **33**, 2731 (1971).
(60) H. Kudo, H. Muramatsu, H. Nakahara, K. Miyano, and I. Kohno, Phys. Rev. C **25**, 3011 (1982).
(61) J. R. Boyce, T. D. Hayward, R. Bass, H. W. Newson, E. G. Bilpuch, F. O. Purser, and H. W. Schmitt, Phys. Rev. C **10**, 231 (1974).
(62) C. J. Bishop, R. Vandenbosh, R. Aley, R. W. Shaw, Jr., and I. Halpern, Nucl. Phys. A **150**, 129 (1970).
(63) M. Strecker, R. Wien, P. Plischke, and W. Scobel, Phys. Rev. C **41**, 2172 (1990).
(64) I. Nishinaka : private communication.
(65) A. H. Wapstra, G. Audi, and R. Hoekstra, At. Data Nucl. Data Tables **39**, 281 (1988).
(66) J. Jänecke and P. J. Masson, At. Data Nucl. Data Tables **39**, 265 (1988).
(67) B. D. Wilkins, E. P. Steinberg, and R. R. Chasman, Phys. Rev. C **14**, 1832 (1976).
(68) S. Goto, D. Kaji, H. Kudo, M. Fujita, T. Shinozuka, and M. Fujioka, J. Radioanal. Nucl. Chem. **239**, 109 (1999).
(69) Ph. Quentin, J. Phys. (Paris) **7**, 32 (1969).
(70) U. Brossa, S. Grossmann, and A. Müller, Phys. Rep. **197**, 402 (1990).
(71) I. F. Croall and J. G. Cuninghame, Nucl. Phys. A **125**, 402 (1969).